Octobre 1982 INT 108/82

OPTICAL FILTERING TECHNIQUES APPLIED TO THE STUDY OF COLLECTIVE DENSITY FLUCTUATIONS IN PLASMAS

Proposal for a new diagnostic

Henri WEISEN

Centre de Recherches en Physique des Plasmas
Association Euratom - Confédération Suisse
Ecole Polytechnique Fédérale de Lausanne

INTRODUCTION

Schlieren and related techniques have been successfully applied to plasmas of relatively high density using visible light [12]. They are based on light deflexion by an electron density gradient. They are limited by a basic uncertainty relation between position and angle of deflexion. It leads to untolerable uncertainties for tokamak conditions, independently of the wavelength used [13].

This situation called for another pair of observable quantities, which are not subject to the uncertainty mentioned: position and (relative) phase. Thus optical filtering methods were considered, which may sometimes appear as being just new interpretations of old techniques. The main difference is that instead of being limited by diffraction, they are based on diffraction.

The most promising technique, phase contrast, has been applied to plasmas by Presby and Finkelstein, with a huge increase in sensitivity over Schlieren techniques, using a pulsed ruby laser [14].

We investigated if this technique could be applied to tokamaks using a pulsed D_2O laser. The answer was essentially negative, for reasons that are beyond the scope of this report. Time resolved observation using a CW laser released many conflicting constraints.

The aim of the present report is to propose methods of real-time observation of plasma density fluctuations based on optical filtering. Their sensitivity is adequate for the study of collective fluctuations that are known to exist in tokamaks. They could contribute considerably to the understanding of the turbulent behaviour of plasmas.

The first four chapters deal with optical field propagation. The reader who is less interested in optics may read chapter II only. Chapter V is about sensitivity and chapter VI presents the various possibilities offered by optical filtering methods. A first experiment is presented in appendix A1.

CONTENT

I. DIFFRACTION

We present a shorthand description of scalar optical field propagation through free space and optical elements along the lines of réf. [1]. The fields resulting from propagation through any optical instrument are expressed as the output of linear (and often shift invariant) systems.

The monochromatic fields shall be represented by their phasors or complex amplitudes, thus we are dropping their monochromatic time dependence.

$$u(\underline{x},t) = A(\underline{x},t)\exp\{i2\pi\nu_0 t\}$$

The validity of using time dependent complex amplitudes is limited to frequencies much below optical frequencies and will be discussed later. A rigorous treatment of scalar diffraction has been given by Kirchhoff, 1882 [2]. In the present context, restriction to the following elementary statements is adequate:

a) The wave equation is satisfied by plane waves satisfying the dispersion relation of the medium.
b) Any physically realizable optical field may be expressed as a linear superposition of plane waves, thus possesses a Fourier transform.
c) A point source produces a spherical wave.

1.1 Free propagation

In the present section we derive the relationship between the complex amplitude distributions at two parallel planes. $\underline{x} = (x_1, x_2)$ is the coordinate in the planes and z the coordinate perpendicular to them. The optical wavefield propagates from a plane located at $z = z_1$ to a plane located at $z = z_2$. We wish to find the impulse response and the transfer function describing this propagation.

a) General expressions

A point source can be represented by

$$a_1(\underline{x}) = \delta(\underline{x})$$

where the suffix 1 designates the location of the plane at $z = z_1$. The corresponding field $A_2(\underline{x})$ at $z = z_2$, the impulse response of the system, is a spherical wave field :

$$a_2(\underline{x}) = h_{12}(\underline{x}) \equiv \frac{\exp\left\{ik_0 z_{12}\left(1+\frac{\underline{x}^2}{z_{12}^2}\right)^{1/2}\right\}}{i\lambda z_{12}\left(1+\frac{\underline{x}^2}{z_{12}^2}\right)} \qquad (1.1)$$

where $z_{12} = z_2 - z_1$

and $k_0 = 2\pi/\lambda$ is the wave number

A general optical field $A_2(\underline{x})$ can be obtained by convolution:

$$A_2(\underline{x}) = h_{12}(\underline{x}) \otimes A_1(\underline{x})$$

$$= \frac{1}{i\lambda z_{12}} \int A_1(\underline{\alpha}) \frac{\exp\left\{ik_0 z_{12}\left(1+\frac{|\underline{x}-\underline{\alpha}|^2}{z_{12}^2}\right)^{1/2}\right\}}{\left(1+\frac{|\underline{x}-\underline{\alpha}|^2}{z_{12}^2}\right)} d\alpha_1 d\alpha_2$$

This is a slight approximation of the Kirchhoff diffraction formula where obliquity factors are ignored [2].

The corresponding transfer function is found by examining the propagation of plane waves :

$$A_z(\underline{x}) = A_0 \exp\{ik_{0z} z\} \exp\{i\underline{k}_{0x}\underline{x} + \phi\}$$

The Fourier transform (over x_1 and x_2) of that field is

$$\tilde{A}_z(\underline{k}) = A_0 \exp i\{k_{0z} z + \phi\} \delta(\underline{k} - \underline{k}_{0x})$$

where $\underline{k}_o = (k_{ox_1}, k_{ox_2}, k_{oz}) = (\underline{k}_{ox}, k_{oz})$

and $k_o^2 = |\underline{k}_{ox}|^2 + k_{oz}^2$

The transfer function simply appears to be

$$H_{12}(\underline{k}) = \frac{\tilde{A}_{z_2}(\underline{k})}{\tilde{A}_{z_1}(\underline{k})} = \exp\{i k_z z_{12}\}$$

$$H_{12}(\underline{k}) = \exp\left\{i z_{12} k_o \sqrt{1 - \frac{\underline{k}^2}{k_o^2}}\right\} \qquad (1.2)$$

b) Fresnel approximation

The Fresnel approximation is useful to analyze optical systems. It is essentially a quadratic approximation of the phase terms of both the impulse response and the transfer function

$$h_{12}(\underline{x}) = (i\lambda z_{12})^{-1} \exp\left\{i k_o z_{12} \left(1 + \frac{\underline{x}^2}{2 z_{12}^2}\right)\right\} \qquad (1.3)$$

$$H_{12}(\underline{k}) = \exp\left\{i k_o z_{12} \left(1 - \frac{\underline{k}^2}{2 k_o^2}\right)\right\} \qquad (1.4)$$

These expressions are easily seen to be Fourier transforms. The approximations are valid when the error on the phase term is considerably smaller than a radian.

For the impulse response, considering the term of order 4 in the Taylor expansion of the square root, this condition yields :

$$z_{12}^3 \gg \frac{\pi (L_1 + L_2)^4}{4\lambda}$$

where L_1 is the extent (radius) around the z axis from which radiation is emitted (for example clear aperture of radius L_1) and L_2 the extent over which radiation is collected. For the transfer function, the Fresnel condition reads :

$$(k/k_0)^4 \ll 4\lambda/\pi z_{12}$$

Using the identity

$$f(\underline{x}) \otimes \exp\{ia\underline{x}^2\} = \exp\{ia\underline{x}^2\}\, TF\left[f(\underline{x})\exp\{ia\underline{x}^2\}\right]\Big|_{\underline{k}=a\underline{x}} \qquad (1.5)$$

we may express the Fresnel integral as

$$A_2(\underline{x}) = \frac{e^{ik_0 z_{12}}}{i\lambda z_{12}} \exp\{i\frac{k_0\underline{x}^2}{2z_{12}}\}\, TF\left[A_1(\underline{x})\exp\{i\frac{k_0\underline{x}^2}{2z_{12}^2}\}\right]\Big|_{\underline{k}=\frac{\underline{x}k_0}{z_{12}}} \qquad (1.6)$$

where $TF[f(\underline{x})] = \tilde{F}(\underline{k})$ is the Fourier transform of f(x).

c) Fraunhofer approximation

Expanding $\exp\{ik_0x^2/2z_{12}\}$ we obtain

$$\exp\{i\frac{k_0\underline{x}^2}{2z_{12}}\} = 1 + i\frac{k_0\underline{x}^2}{2z_{12}} - \frac{1}{2}\left(\frac{k_0\underline{x}^2}{2z_{12}}\right)^2 + \ldots \qquad (1.7)$$

The Fraunhofer approximation consists in using the approximation of order 0 in (1.6)

$$A_2(\underline{x}) = \frac{e^{ik_0 z_{12}}}{i\lambda z_{12}}\, TF\left[A_1(\underline{x})\right]\Big|_{\underline{k}=\frac{\underline{x}k_0}{z_{12}}} \qquad (1.8)$$

The Fraunhofer (or far-field) approximation is valid for

$$|z_{12}| \gg \frac{\pi L_1^2}{\lambda} \quad \text{and} \quad L_2^4 \ll \frac{4\lambda |z_{12}|^3}{\pi}$$

the Fresnel and Fraunhofer conditions can be released when the observation is not constrained to the plane at $z = z_2$, but to a spherical surface of radius z_{12} centered at $(0, 0, z_1)$.

1.2 The effect of lenses on diffraction

An ideal lens converts an incident spherical wave into another spherical wave :

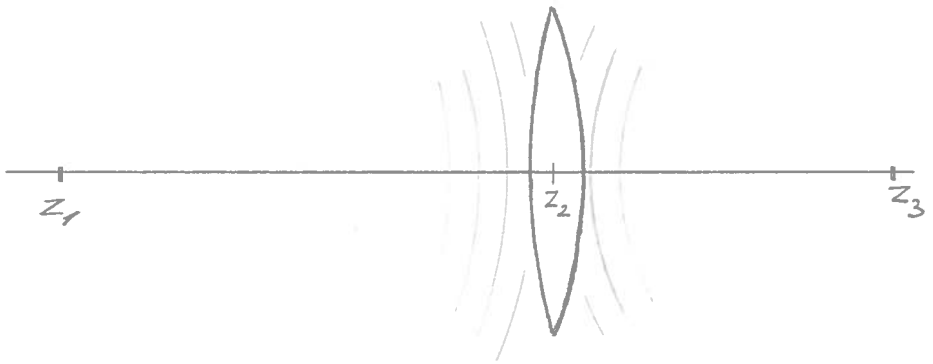

Fig. 1.1

In the Fresnel approximation the incident field is

$$A_2(\underline{x}) = A_0 \exp\left\{ i \frac{k_0 \underline{x}^2}{2 z_{12}} \right\}$$

and the field "behind" the lens

$$A_2'(\underline{x}) = A_0 P(\underline{x}) \exp\left\{ -i \frac{k_0 \underline{x}^2}{2 z_{23}} \right\}$$

where $P(\underline{x})$ is a pupil function (aperture).
The complex amplitude transmittance of this lens is thus

$$t(\underline{x}) \equiv \frac{A_2'(\underline{x})}{A_2(\underline{x})} = P(\underline{x}) \exp\left\{ -i \frac{k_0 \underline{x}^2}{2f} \right\} \qquad (1.9)$$

where f is called the focal length of the lens and is defined by

$$\frac{1}{f} = \frac{1}{z_{12}} + \frac{1}{z_{23}} \qquad (1.10)$$

a) Image formation by a lens

We wish to calculate the impulse response and the transfer function for the propagation between the planes $z = z_1$ and $z = z_3$, with a lens located at z_2 (Fig. 1.1).

$$A_1(\underline{x}) = S(\underline{x} - \underline{x}_0)$$

$$A_2(\underline{x}) = h_{12}(\underline{x} - \underline{x}_0)$$

$$A_2'(\underline{x}) = h_{12}(\underline{x} - \underline{x}_0) \exp\left\{-i \frac{k_0 \underline{x}^2}{2f}\right\} P(\underline{x})$$

$$= B_{12} \exp i\left\{-\frac{k_0 \underline{x}\,\underline{x}_0}{z_{12}} + \frac{k_0 \underline{x}_0^2}{2z_{12}} - \frac{k_0 \underline{x}^2}{2z_{23}}\right\} P(\underline{x})$$

Here (1.10) was used to eliminate a reference to f. The first term in the exponential describes a phase shift which is linear in $\underline{x}$ and $\underline{x}_0$ and the last term a wavefield which is converging towards z_3.

$B_{ij} = (i\lambda z_{ij})^{-1} \exp(i k_0 z_{ij})$

Propagation from z_2 to z_3 is described by (1.3) and (1.6) :

$$A_3(\underline{x}) = A_2'(\underline{x}) \otimes h_{23}(\underline{x})$$

$$= B_{12} B_{23} \exp\left(i \frac{k_0 \underline{x}^2}{2z_{12}}\right) \left\{\exp\left(-i \frac{k_0 \underline{x}\,\underline{x}_0}{z_{12}} - i \frac{k_0 \underline{x}^2}{2z_{23}}\right) P(\underline{x}) \otimes \exp\left(i \frac{k_0 \underline{x}^2}{2z_{23}}\right)\right\}$$

$$= B \exp\left(i \frac{k_0 \underline{x}^2}{2z_{23}}\right) TF\left[\exp\left(-i \frac{k_0 \underline{x}\,\underline{x}_0}{z_{12}}\right) P(\underline{x})\right]\Big|_{\underline{\xi} = \frac{\underline{x} k_0}{z_{23}}}$$

$$= B \exp\left(i \frac{k_0 \underline{x}^2}{2z_{23}}\right) \tilde{P}\left(\frac{\left(\underline{x} + \frac{\underline{x}_0 z_{23}}{z_{12}}\right) k_0}{z_{23}}\right) \qquad (1.11)$$

$$\equiv h_{13}^{\ell}(\underline{x} - \underline{x}_0)$$

where $B = B_{12} B_{23} \exp\left(i \frac{k_0 x_0^2}{2 z_{12}}\right)$

From (1.11) we deduce :

- The lens produces an inverted image, with magnification $m = -z_{23}/z_{12}$

- The impulse response is proportional to the Fourier transform of the pupil function, a spatial frequency $\underline{k}$ appears at $\underline{x} = z_{23} \underline{k} / k_0$

Strictly speaking the presence of the quadratic phase factor $\exp\left(i \frac{k_0 x^2}{z_{23}}\right)$ suggests that the Fourier transform is found on a spherical surface of radius z_{23} centered at z_2. Similarly, shift invariance for P is found between this sphere and a sphere of radius z_{12} centered at z_2. The quadratic phase factors are however of little practical importance and are usually ignored. The transfer function is a scaled version of the pupil function. This can be seen from the Fourier transform of the impulse response.

$$H^{\ell}_{13}(\underline{k}) = \tilde{P}\left(-\frac{\underline{k} z_{23}}{k_0}\right) \qquad (1.12)$$

b) Fourier transform by a lens

As we made no particular assumption concerning the pupil function, the result (1.11) remains valid if the pupil contains a partially transparent object with complex amplitude transmittance $t(\underline{x})$. We just need to replace $P(\underline{x})$ by

$$P(x) = C(x)\, t(x)$$

where $C(\underline{x})$ is a clear aperture (1 inside, 0 outside); we get

$$A_3(x) = B \exp\left(i \frac{k_0 x^2}{2 z_{23}}\right) \left[\tilde{C}_{\left(\frac{x k_0}{z_{23}}\right)} \otimes \tilde{T}_{\left(\frac{x k_0}{z_{23}}\right)}\right] \qquad (1.11\text{bis})$$

where $T(\underline{k})$ is the Fourier transform of $t(\underline{x})$. This situation may be obtained by placing the transparency just in front or just behind the lens. Eq. (1.11bis) can easily be generalized for a transparency illuminated by a converging wavefield, where z_{23} is the distance from the transparency to its center of curvature. The convolution operation in (1.11bis) represents a limit of the spectral resolution, since the width of $C(\underline{k})$ in $\underline{k}$-space is of the order of 1/D, where D is the diameter of the aperture. Thus two spatial frequencies present in the object have to differ by a few periods over the whole aperture in order to be separated.

The calculation of the diffraction pattern at z_3 is much more intricate when the object is located at z_0 in front of the lens.

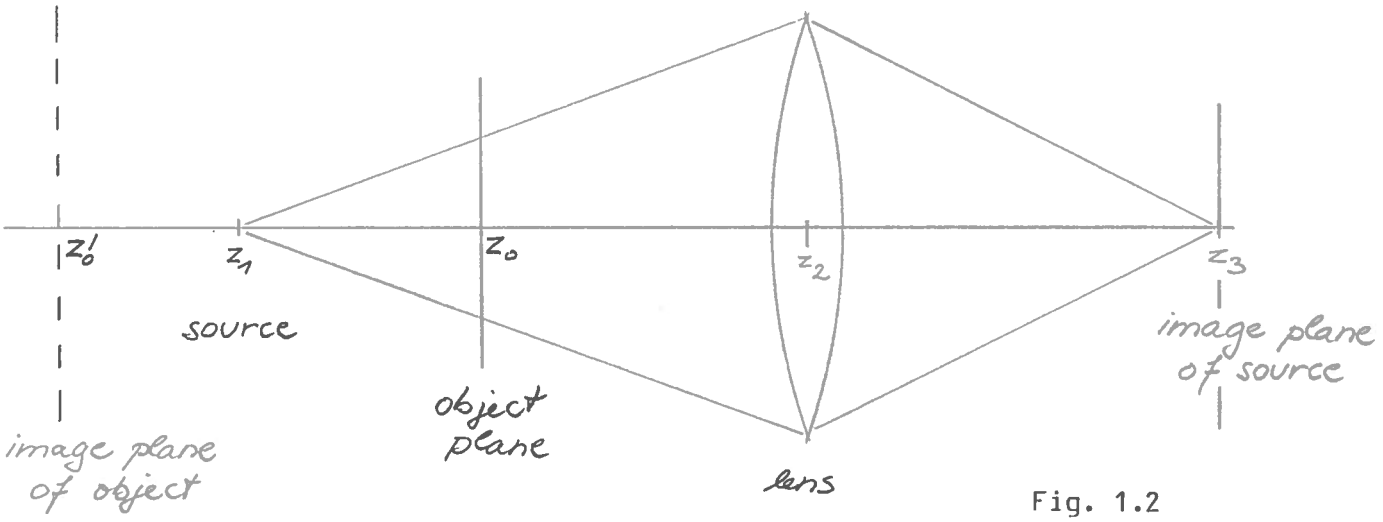

Fig. 1.2

Gaskill [1], assuming all of the diffracted light is collected by the lens, finds

$$A_3(\underline{x}) = B_{10} B_{02} B_{23} \exp(ik_0 z_{02}) \exp\left\{ i \frac{k_0 \underline{x}^2}{2 z_{23}} \left(1 - \frac{z_{12} z_{02}}{z_{10} z_{23}}\right)\right\} \tilde{T}\left(\frac{\underline{x}\, k_0 z_{12}}{z_{10} z_{23}} \right) \qquad (1.11ter)$$

Thus a spatial frequency $\underline{k}$ appears at

$$\underline{x}(\underline{k}) = \frac{z_{10} z_{23}}{z_{12}} \frac{\underline{k}}{k_0} \qquad (1.13)$$

This result may be understood as follows. The lens produces a magnified image of the object at a plane z_0' (Fig. 1.2) and the system behaves as if this image was illuminated by a wave converging towards z_3. The distance

$$z_{0'3} + z_{23} = z_{23}\left(1 - \frac{z_{12}\, z_{02}}{z_{10}\, z_{23}}\right)^{-1}$$

explains the quadratic phase factor. The magnification of the image is $m = (z_{03} - z_{23}) / z_{02}$, so that the scaling factor for the Fourier transform is found to be

$$\frac{m}{z_{0'3}} = \frac{z_{12}}{z_{10}\, z_{23}}$$

A special case is obtained when the object is located at the front focal plane, defined by $z_{02} = f$, because the quadratic phase factor then vanishes. If, moreover we illuminate the transparency with a plane wave ($z_{12}/z_{10} \longrightarrow 1$, $z_{12} \longrightarrow \infty$), we get rid of any reference to the incident wave :

$$A_3(\underline{x}) \propto \tilde{T}\left(\frac{\underline{x}\, R_0}{f}\right)$$

Since we may now take $t(\underline{x})$ to be the complex amplitude in $z = z_0$, we conclude that a lens produces in its back focal plane (defined by $z_{23} = f$) a complex amplitude distribution that is the Fourier transform of the amplitude in its front focal plane.

As already pointed out the quadratic phase factor present with other configurations is of little practical relevance. The best performance from the point of view of shift invariance and spectral domain transmitted is obtained by placing the object as close as possible to the lens.

II. OPTICAL FILTERING

The next step is to act on the spatial spectrum of the object, to apply an inverse Fourier transform and get a filtered version of the complex amplitude transmittance of the object. The inverse transform may be produced either by a second lens or by free propagration of a converging wave-field. The latter will be discussed in Appendix 1.

For the two-lens-systems there exists a great variety of cases, depending on source and object locations with respect to the lenses treated in great detail by [1].

An interesting case is when the two lenses are separated by the sum of their focal lengths. The image magnification is independent of the object location and equal to the ratio of the focal lengths. This is an advantage if the object has a considerable spatial depth, or its position is not always the same, because focussing can be changed without change of magnification by moving the observation plane.

2.1 Formalism

The "4f setup" is a special case where the two focal lengths are equal (Fig. 1.3). Object and image plane are then always separated by a distance equal to 4f. Parallel illumination makes the analysis of the system easier (especially for deep objects) but is not a necessary condition, neither is the exact location of the object in a focal plane.

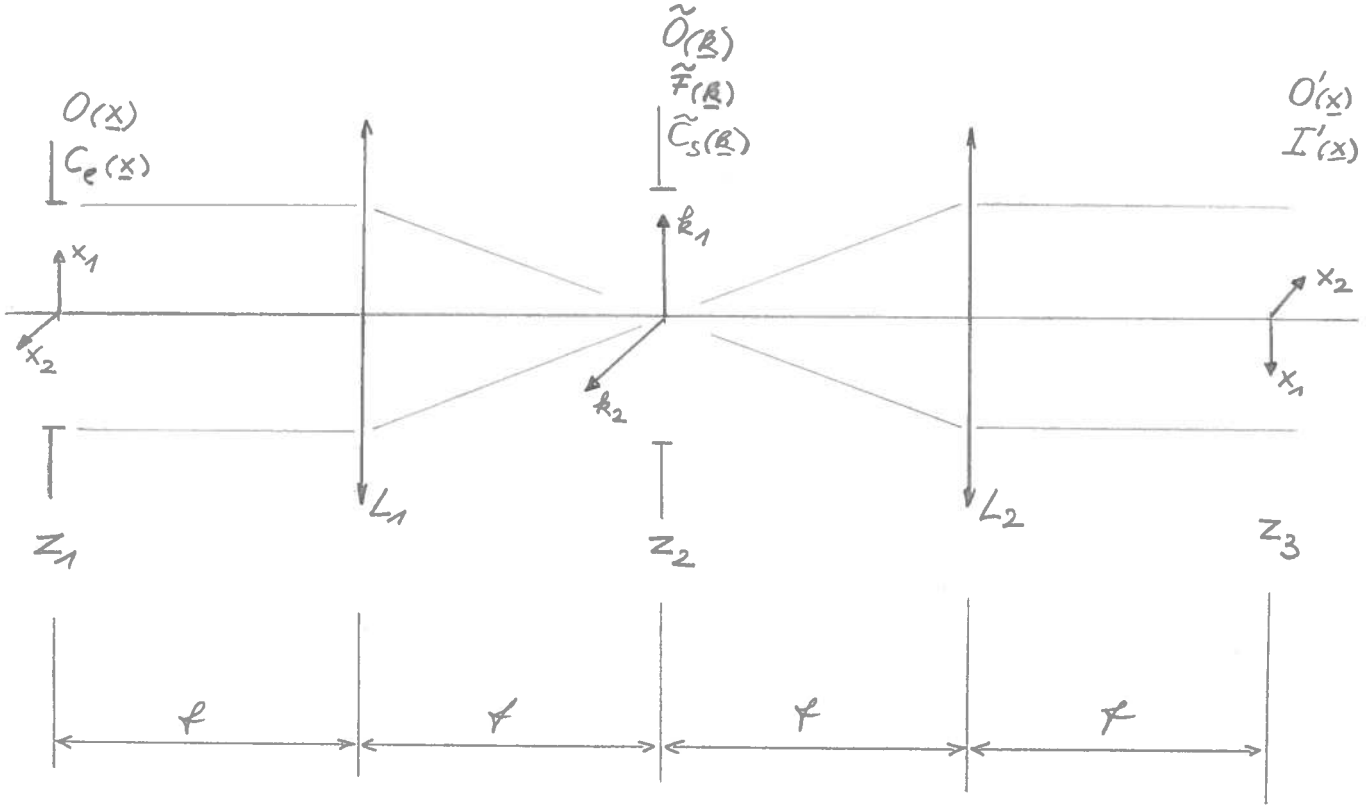

Fig. 1.3

Fig. 1.3 should therefore be understood as the formal equivalent-apart from considerations concerning magnification and scaling factors - of any shift invariant optical filter, not necessarily as a design proposal.

The object is located in plane z_1, its sepctrum is displayed in plane z_2. Lens L_2 produces a second Fourier transform. In optics the usual convention of orientation of the axis in plane z_3 allows us to consider it as an inverse transform - keeping in mind that the image is inverted. The aperture functions $C_1(\underline{x})$ and $\tilde{C}_s(\underline{k})$ are positioned at their unusual locations for formal convenience. The lenses are supposed to transmit all of the diffracted light.

The amplitude at plane z_1 is

$$O(\underline{x}) = t(\underline{x})\, C_e(\underline{x})$$

The amplitude at z_2 :

$$\tilde{O}_{(\underline{k})} = \tilde{T}_{(\underline{k})} \otimes \tilde{C}_{e\,(\underline{k})} \tag{2.1}$$

A filter of complex amplitude transmittance $\tilde{F}(\underline{k})$ is located in the Fourier plane, yielding :

$$\tilde{O}'_{(\underline{k})} = \tilde{C}_{s\,(\underline{k})}\, \tilde{F}_{(\underline{k})} \left[\tilde{T}_{(\underline{k})} \otimes \tilde{C}_{e\,(\underline{k})} \right] \tag{2.1'}$$

At the image plane we obtain the inverse transform of $\tilde{O}'(\underline{k})$:

$$O'_{(\underline{x})} = c_{e(\underline{x})}\, t_{(\underline{x})} \otimes f_{(\underline{x})} \otimes c_{s\,(\underline{x})} \tag{2.2}$$

where

$$f_{(\underline{x})} = TF^{-1}\left[\tilde{F}_{(\underline{k})} \right]$$

$$c_{s(\underline{x})} = TF^{-1}\left[\tilde{C}_{s\,(\underline{k})} \right]$$

The system thus has an impulse response

$$h_{(\underline{x})} = f_{(\underline{x})} \otimes c_{s\,(\underline{x})} \tag{2.3}$$

and a transfer function

$$H_{(\underline{k})} = \tilde{F}_{(\underline{k})}\, \tilde{C}_{s(\underline{k})} \tag{2.4}$$

For a circular aperture of diameter d_s we have

$$c_{s(\underline{x})} = \frac{d_s}{2|x|} J_1\left(\frac{\pi |x| d_s}{\lambda f} \right) \tag{2.5}$$

Discussion

In a setup where the object is close to L_1 and the Fourier plane close to L_2 the physical significance of $C_e(\underline{x})$ and $C_s(\underline{k})$ is obvious (aperture of lenses or illuminated area). When these distances are increased as is often necessary this significance holds only for objects of limited extent around the z-axis or objects with limited spatial frequency content. (The degree of shift invariance is reduced). One may identify to some extent $C_e(\underline{x})$ with the physical aperture of L_1 and $C_s(\underline{x})$ with the most limiting element of L_1 and L_2.

The simplest filters one can imagine are masks obstructing a domain in $\underline{k}$-space. Strioscopy for example uses a central stop to eliminate undiffracted light and form an image with diffracted light only.

2.2 Phase contrast

a) Principle

Phase contrast is a technique which makes possible the visualization of phase objects introducing phase shifts much smaller than a radian.

A thin phase object can be described by its complex amplitude transmittance, and for small phase shifts approximated as follows :

$$t(\underline{x}) = \exp\{i\varphi(\underline{x})\} \simeq 1 + i\varphi(\underline{x}) \qquad (2.6)$$

Thus the object separates the incident light into two parts, a diffracted and an undiffracted part. It must be emphasized that $\phi(\underline{x})$ describes only phase shifts with respect to the undiffracted light, e.g. the continuous component of the optical signal. It describes deformations of the wavefronts as they traverse the object. The spectrum of this signal from (2.1) :

$$\tilde{O}_{(\underline{k})} = \tilde{C}_{e(\underline{k})} + i\tilde{\varphi}_{(\underline{k})} \otimes \tilde{C}_{e(\underline{k})} \qquad (2.7)$$

As diffracted and undiffracted light are in phase quadrature (phase difference $\pi/2$), the resulting intensity in the object plane is uniform. The phase contrast method "corrects" this situation by phase shifting the diffracted light by $\pm\ \pi/2$ with respect to the undiffracted light using a central phase plate of suitable optical thickness. To improve the contrast the background illumination is reduced by attenuating the undiffracted light.

Ideally the transmitted spectrum would be :

$$\tilde{O}_{(\underline{k})} = \left[\theta\tilde{C}_{e(\underline{k})} + \tilde{\varphi}_{(\underline{k})} \otimes \tilde{C}_{e(\underline{k})}\right] C_{S(\underline{k})} \qquad (2.8)$$

and the amplitude in the image plane :

$$O'_{(\underline{x})} = \left(\theta + \varphi_{(\underline{x})}\right) . C_{e(\underline{x})} \otimes C_{S(\underline{x})} \qquad (2.9)$$

Within the resolution capabilities of the system the intensity is thus

$$I'_{(\underline{x})} = \theta^2 + 2\theta\varphi_{(\underline{x})} + \varphi^2_{(\underline{x})} \qquad (2.10)$$

When the photodetector has a limited dynamical range (eye, photographic emulsion) contrast is optimised by setting $\theta \gg |\varphi(\underline{x})|$. In other cases it may be more interesting to maximise the useful signal - $2\theta\,\varphi(\underline{x})$ - by setting θ equal to 1 :

$$I'_{(\underline{x})} \simeq 1 + 2\varphi_{(\underline{x})} \qquad (2.11)$$

If the phase shift is not equal to π, but equal to ν, 2.10 becomes

$$I'_{(\underline{x})} = \theta^2 + 2\sin\nu\,\theta\,\varphi_{(\underline{x})} + \varphi^2_{(\underline{x})} \qquad (2.12)$$

b) Optical performance

If the non attenuating phase plate has a physical diameter D, the transfer function of the system is

$$H(\underline{k}) = \begin{cases} i & \text{for } |k| < k_c = D/2fk_0 \\ 1 & \text{for } d_s/2fk_0 < |k| < D/2fk_0 \end{cases}$$

where d_s is the physical diameter associated with $C_s/\underline{k}$. Only spatial frequencies between D/fk_0 and d_s/fk_0 will be revealed; the instrument is a pass-band.

In order to increase the bandwidth at the low frequency side we may take D approximately equal to the diameter of the Airy disk

$$D = 1.2\,\lambda f/d_e$$

where d_e is the physical diameter associated with $C_e(\underline{x})$ the cutoff frequency is then

$$k_c \simeq 5/d_e$$

As an example a sinusoidal phase object of spatial frequency k will be well reproduced when most of its spectrum lies outside the phase plate. As it is itself diffraction broadened by $5/d_e$ this is the case for

$$k \gtrsim 2k_c \simeq 10/d_e$$

or

$$\Lambda \lesssim \frac{2\pi d_e}{10} \simeq 2/3\, d \qquad (2.13)$$

where Λ is the period of the object. We must conclude that the diameter of the incident beam, and thus the collecting optics must be at least 1.5 times larger than the wavelength we wish to observe. This result holds only for diffraction limited focussing of the collected radiation. The bandwidth at the low k side is decreased proportionnally to the increase of the central spot size by aberrations.

c) Background homogeneity

In absence of an object the original background distribution is not conserved. As is easily seen the intensity in the image plane consists of the sum of the intensities of a low pass version and a high pass version of the original background field, the cutoff frequency being k_c. Background modulations are present and may limit considerably the observation of small phase shifts, especially if the cutoff frequency is low. The exact amplitude depends on the beam profile and may be reduced by apodisation (gaussian beam). Numerical simulations of a phase contrast system showed that even in the precence of modulations at the 10% level the original phase perturbation could be obtained by subtraction of the background. This is however not the approach of the present report where time dependent observation is proposed. Spatial inhomogeneity being stationnary, it just provides a (slightly) different DC signal at different points. The DC signal is filtered off.

Thus for the case envisaged there are no particular requirements on background homogeneity that could conflict with optical performance at low k.

2.3 Application to plasma physics

a) Plasma refractivity

From the dispersion relation for transverse waves in a plasma

$$\omega^2 = \omega_{pe}^2 + c^2 k^2$$

we find for $\omega^2 >> \omega^2_{pe}$ the refractive index given by

$$n = 1 - \frac{\omega_{pe}^2}{2\omega^2} = 1 - \frac{e^2 \lambda^2 n_e}{2\pi m_e c^2} \qquad (2.14)$$

where n_e is the electron density, c the speed of light, e the electronic charge, ω_{pe} the electron plasma frequency and ω the frequency of the wave. In the thin object model, the phase-shift with respect to vacuum experienced by an electromagnetic wave is proportional to the traversed electron thickness $N(\underline{x})$:

$$\varphi(\underline{x}) = -2\pi\lambda \cdot 4.48 \cdot 10^{-14} N(\underline{x}) \qquad (c.g.s)$$

where $$N(\underline{x}) = \int n_e(\underline{x}, z)\, dz \qquad (2.15)$$

To give an order of magnitude, at $\lambda = 10.6\ \mu$ (CO_2) the total electron thickness at the center of the plasma of TCA gives rise to phase-shifts of the order of 0.3 radians and $\sim$ 12 radians at $\lambda = 383\ \mu$ (D_2O). As we wish to detect fluctuations of the order $\Delta n_e/n_e \simeq$ 1% which might be found within a depth of only 1/10 of the total plasma diameter, the phase shifts to be detected are of the order of $3 \cdot 10^{-4}$ radians for an IR and 10^{-2} radians for an FIR source.

Previous studies of instantaneous imaging showed that the dynamical range of detectors is insufficient in the IR whereas background inhomogeneities due to the slowly varying but important overall plasma optical thickness would be the limiting factor in the FIR.

b) Time resolved observation

The only way to overcome these porblems appeared to be temporal observation with a single element detector of high dynamical range and fast response like a photovoltaic diode. The attraction of a 2D-image of the plasma is thus lost in favor of temporal, but still spatially resolved information. The advantage of 2D observation can be partially recovered by the use of detector arrays.

Temporal observation opens new perspectives : By selecting a given spatial frequency domain dispersion relations can be obtained, but we can also record the whole diffracted (ω-) spectrum at once, at a given image point. Two or more detectors permit spatio-temporel correlations. The activity of selected modes (by $\underline{k}$ and $\underline{\omega}$) can be followed in space and time. This approach appears to be more interesting and usefull from a plasma physics point of view than the original idea of instantaneous imaging.

Before we calculate the sensitivity of such an instrument, we have to consider two special problems associated with the application of optical filtering to the detection of plasma fluctuatiosn:

1) Validity of the concept of complex amplitude in a non stationnary context.

2) Validity of the thin object model for an extended plasma.

III. TIME DEPENDENT COMPLEX AMPLITUDE

When a monochromatic wave interacts with a non stationnary object, the resulting wave is either not monochromatic, or shifted in frequency. We may however express the transmitted wave-field as a superposition of plane waves of the form

$$A(\underline{x},t) = A_0 \exp\{i(\underline{k}\underline{x} - \omega t)\}$$

here $\underline{x} = (x_1, x_2, x_3)$; $\underline{k} = (k_1, k_2, k_3)$

obeying the dispersion relation (vacuum)

$$\omega^2 = k^2 c^2$$

We may express $A(\underline{x}, t)$ with reference to the incident wave of wave-vector $\underline{k}_0$ and frequency ω_0.

$$A(\underline{x},t) = A_0 \exp\{i(\Delta\underline{k}\,\underline{x} - \Delta\omega t)\} \exp\{i(\underline{k}_0\underline{x} - \omega_0 t + \phi)\}$$

For $||k| - |k_0|| \ll 1$ the propagation properties of the resulting wave are well described by those of the incident wave. We may thus (for $\Delta\omega \ll \omega$) interpret the $\exp\{-i\Delta\omega t\}$ term as the time dependent part of the complex amplitude.

For an experiment based on a praticular phase relationship between several wavefields (e.g. phase contrast) we have to consider the effect of the phase-term in $\Delta\underline{k}\underline{x}$ equal to $\Delta k_{//} x$ when $\underline{x} // \underline{k}$. From the dispersion relation we find

$$\Delta k_{//} x = \Delta\omega x / c$$

Thus, because of the frequency shift $\Delta\omega$, the diffracted wave experiences an additional phase shift as it propagates, due to a slight change in its wavenumber.

To avoid an influence on the phase we must require

$$\Delta\omega \ll c/\ell \qquad (3.1)$$

where l is the distance from the disturbance to the observation plane. For a distance of 2 meters this yields :

$$\frac{\Delta\omega}{2\pi} \ll 25\ MHz$$

Most of the density fluctuations we expect to detect with phase contrast satisfy this condition. At higher frequencies simultaneous compensation is only possible for a limited range of frequencies. The simplest solution to this problem is to produce an image with only one order of diffraction at frequencies above a few MHz.

IV. THICK OBJECTS

4.1 Depth of focus

As a first approach to determine the acceptable depth of field we analyze the effect of the focussing error on a thin plane wave situated at a distance z_{12} to the plane of observation.

$$\varphi(\underline{x}) = \varphi_0 \sin(\underline{\alpha}\,\underline{x}) \qquad \underline{x} = (x_1, x_2)$$

$$A_1(\underline{x}) = 1 + i\,\varphi_0 \sin(\underline{\alpha}\,\underline{x})$$

$$A_2(\underline{x}) = A_1(\underline{x}) \otimes h_{12}(\underline{x})$$

$$= 1 + \varphi_0 \sin(\underline{\alpha}\,\underline{x}) \exp i\left\{\frac{\pi}{2} - \frac{z_{12}\underline{\alpha}^2}{2k_0}\right\}$$

$$I_2(x) = 1 + 2\varphi_0 \sin(\underline{\alpha}\,\underline{x}) \sin\left(\frac{z_{12}\underline{\alpha}^2}{2k_0}\right) + O(\varphi_0^2)$$

$A_2(\underline{x})$ is the amplitude in the focal plane of the optics. There is an offset from quadrature between diffracted and undiffracted wave by the phase factor $\Delta z k^2/2k_0$. In the expression (2.12) we thus have $\nu = \pi/2 - \Delta z k^2/2k_0$. We arbitrarily define the maximum acceptable focussing error for phase contrast as the distance causing the mixing term of (2.12) to be 70% of its infocus value:

$$z_{12\,max} = \frac{\pi}{2}\frac{k_0}{k^2} = \frac{1}{4}\frac{\Lambda^2}{\lambda} \qquad (4.1)$$

where $\Lambda = 2\pi/k$ and $\lambda = 2\pi/k_0$

At CO_2 wavelength the depth of focus is 20 cm for a plasma wavelength above 3 mm, and 4 cm for a plasma wavelength above 1 mm.

The contribution of plane waves outside the depth of focus is difficult to predict because the phase relation between diffracted

undiffracted light may have any arbitrary value. On the other hand contributions from a small object with a broad spatial frequency content can be expected to decrease with increasing defocus.

4.2 Diffraction by a plane wave

Another approach is to investigate the propagation of a plane electromagnetic wave in a medium with a plane wave refractive disturbance [2] :

$$n(x',t) = n_0 + \Delta n \cos(kx' - \omega t)$$

The wave causes refractive index fluctuations of amplitude Δn. It is confined in a region of depth d and propagates in the x' direction (Fig. 4.1). The angle of incidence θ may be different from 0.

Given the weak interactions in a low density plasma we will only consider diffraction of orders ± 1. The diffracted fields are then :

$$u_{\pm 1}(x',y) = V_{\pm 1}(y) \exp i\{(k_0 \sin\theta \pm k)x' - (\omega_0 \pm \omega)t\}$$

The angular separation between orders 1 and 0 is given by:

$$\sin\phi - \sin\theta = \lambda/\Lambda \qquad \text{(grating equation)}$$

$$\text{or} \quad 2\sin\frac{\phi-\theta}{2}\cos\frac{\phi+\theta}{2} = \lambda/\Lambda$$

The diffraction angles $\phi - \theta$ in the optical instruments considered are rather small because of their limited angular acceptance. We may therefore make the following approximations:

$$\phi - \theta \simeq \frac{\lambda}{\Lambda}\frac{1}{\cos\frac{\phi+\theta}{2}} \simeq \frac{\lambda}{\Lambda}\frac{1}{\cos\theta} = \frac{k}{k_0}\frac{1}{\cos\theta} \qquad (4.3)$$

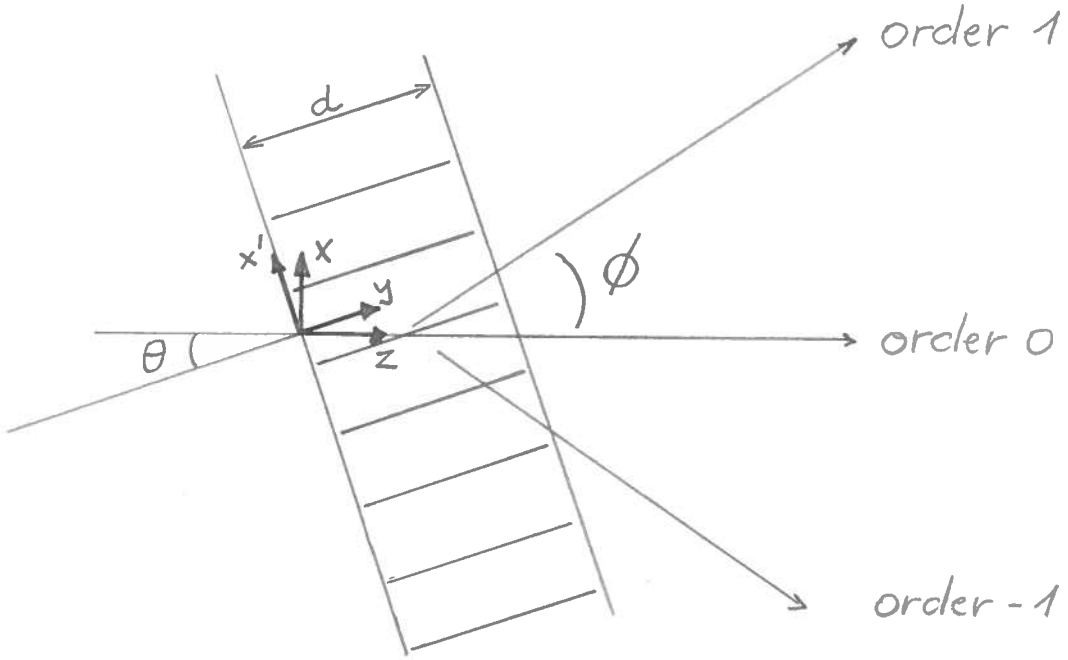

fig. 4.1

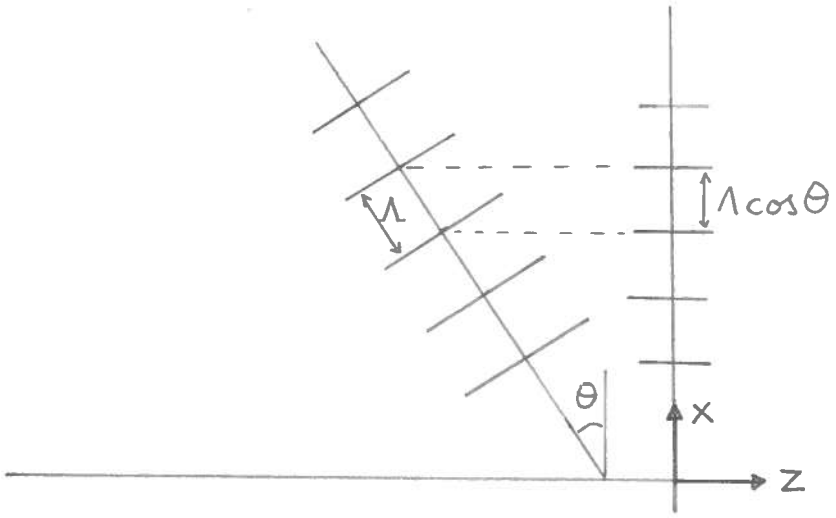

fig. 4.2

The angle of diffraction is the same one would expect from a wave traveling perpendicular to the incident beam, but of wavenumber $k/\cos\theta$ and wavelength $\cos\theta\,\Lambda$ as illustrated by Fig. (4.2)

a) Diffracted amplitudes

From [2] we get for a plane incident field of unit amplitude the following first order approximation :

$$V_{\pm 1}(y) = \Delta n \frac{\Lambda^2}{\lambda^2} \exp\{i\varepsilon(\pi/2 - \beta(\gamma \pm 1/2)y\} \frac{|\sin\{\beta(\gamma \pm 1/2)y\}|}{\gamma \pm 1/2} V_o(y) \quad (4.4)$$

where $V_o(y) = \exp\{i\cos\theta k_o y\}$ is the undiffracted wave

$$\varepsilon = \begin{cases} -1 & \text{if } \beta(\gamma \pm 1/2)y < 0 \\ +1 & \text{if } \beta(\gamma \pm 1/2)y > 0 \end{cases}$$

$$\beta = \frac{\pi\lambda}{\Lambda^2} \qquad \gamma = \frac{\Lambda}{\lambda}\sin\theta$$

n_o is taken to be unit

The quantity β ($\xi \pm 1/2$) is a measure of momentum mismatch between the three wavevectors involved in diffraction. The product of momentum mismatch and interaction depth $d = y_{max}$ determines the diffraction efficiency which in the best case is seen to be limited to

$$|V_{\pm 1}(y)| \leq \Delta n\, \pi d/\lambda \quad (4.5)$$

For a large interaction depth, only the condition $\xi = \mp 1/2$ can ensure optimum diffraction efficiency. This is the Bragg regime where

almost all of the diffracted light is concentrated in a single order. At the other extreme of a relatively short interaction depth we may approach the maximum diffraction efficiency, provided

$$\beta(\zeta \pm 1/2)d \ll 1 \tag{4.6}$$

b) Effective complex amplitude transmittance

We may express (4.2) in terms of the coordinate x, perpendicular to the direction of incidence and obtain "just behind" the object :

$$u_{\pm 1}(x,t) = V_{\pm 1}(d)\, \exp i\{\pm \sin(\phi-\theta) k_0 x \mp \omega t\}\, u_0(x) \tag{4.7}$$

The total transmitted field is

$$u_{tot}(x,t) = u_0(x,t) + \sum_{+,-} u_{\pm 1}(x,t)$$

and may be considered as resulting from an effective complex amplitude transmittance :

$$t(x,t) = 1 + \sum_{+,-} V_{\pm 1(d)} \exp i\{\pm \sin(\phi-\theta) k_0 x \mp \omega t\} \tag{4.8}$$

We may define the thin object regime as the case where both orders are almost in phase quadrature with order 0. This happens when

$$\beta(\zeta+1/2)d \ll 1 \quad \text{or} \quad \beta\zeta d \ll 1 \tag{4.9}$$

and $\beta(\zeta-1/2)d \ll 1$ and $1/2\,\beta d \ll 1$ (4.10)

The second condition agrees within a factor of two with condition (4.1) and leads back to our depth of field consideration. Condition 4.9 sets a limit to the allowed angle of incidence

$$\sin\theta d \ll \Lambda/\pi$$

and simply states the fact that the incident light must not cross successive maxima and minima. In the thin object regime (4.8) leads to the familiar expression

$$t_{(x,t)} = 1 + i\varphi_0 \cos[kx/\cos\theta - \omega t]$$

Where $\varphi_0 = 2\pi\Delta nd/\lambda$ represents a line integral of the refractive index variation accross the interaction region. (compare with page 22)

c) Criteria for diffraction regimes

We may apply the same criterion (4.1) to define a thin object ($|\nu - \pi/2| \leq \pi/4$) :

$$\pi\left(\frac{|\sin\theta|}{\Lambda} + \frac{1}{2}\frac{\lambda}{\Lambda^2}\right)d \ll \pi/4 \qquad (4.11)$$

Graph (4.3) shows the limiting curves d_{max} (Λ) for different values of $\sin\theta$ at CO_2 wavelength. The dotted curves show the allowable depth d when maximum diffraction efficiency is required by

$$\pi\left|\frac{\sin\theta}{\Lambda} + \frac{1}{2}\frac{\lambda}{\Lambda^2}\right|d \ll \pi/4 \qquad (4.12)$$

This condition includes the Bragg regime, appearing as peaks of allowable interaction depth on the left of graph (4.3).

To have a "true" Bragg regime the intensities in opposite orders must be very different (otherwise there is no substantial difference with the thin object regime as defined above). This sets a lower limit to d. We may require that diffraction in the "wrong" order is only due to sidelobes of the $\sin(\beta(\xi \pm 1/2)y)/(\xi \pm 1/2)$ term of (4.4). This leads to the following criterion for a true Bragg regime :

$$\pi\left(\frac{|\sin\theta|}{\Lambda} + \frac{1}{2}\frac{\lambda}{\Lambda^2}\right)d \simeq \pi\frac{\lambda}{\Lambda^2}d \geqslant \pi$$

$$\text{eg.:} \qquad d \geqslant \Lambda^2/\lambda \tag{4.13}$$

d) Discussion

As can be seen from Fig. (4.3) true Bragg regimes will not occur for a plasma wavelength above 2mm when the interaction depth is limited to 30 cm as is the case in most laboratory plasmas (λ = 10.6μ). At a wavelength above 3 mm momentum matching occurs at angles of incidence smaller than $0.15 \cdot 10^2$ radians. At these angles the allowed depth extends already beyond 20 cm.

Thus for wavelength above 3 mm any efficient diffraction is adequately described by the thin object regime, and occurs about equally in orders ±1. For tokamak plasmas this is the range of plasma wavelength where phase contrast can be expected to give the best results. Fortunately most of the expected fluctuations in a tokamak also fall into this range.

Most waves will have a lateral extent d much larger than Λ (Resonant shells may be an important exception). If we set $d \geq 5\Lambda$, which is conservative, we find the region of interest to lie roughly

at the left side of the curve for $\sin\theta = 0.05$ of graph (4.3). Thus the dominant contribution to the observed signals will arise from plasma waves traveling at angles θ less than 0.05 radians to the normal of the optical axis where the $k/\cos\theta$ uncertainty is not too severe (see 4.3).

For $\Lambda < 3$ mm and a large interaction depth or focus uncertainty, the performance of the phase contrast technique is difficult to predict and to interpret. In this range it may be useful to keep only one order of diffraction by using a knife edge (similar to the Schlieren knife edge, but with a hole for order 0) in the Fourier plane. This eliminates the problems of having a fixed phase relationship between orders ± 1 and 0. The output of such a filter would be independent of the regime of diffraction

$$O'(\underline{x},t) = 1 + V_{+1}(d)\exp i\{kx/\cos\theta - \omega t + \phi\}$$

$$I(\underline{x},t) = 1 + 2|V_{+1}(d)|\cos\{kx/\cos\theta - \omega t + \phi\}$$

In the thin object case we get a signal half as intense as for the phase contrast method. The phase of the image of the wave is not identical with the phase of the actual wave. As for phase contrast, however, the sign of the phase velocity can be obtained by correlation measurements using two detectors probing the image field.

Remark

(4.5)-(4.6) might suggest the erroneous conclusion that the basic principle of momentun conservation could be violated "to some extent", particularly in the thin object case. Actually k can be understood as being broadened in a direction perpendicular to the direction of propagation because of the finite lateral extent d of the wave. Diffraction with momentum conservation then occurs from sidebands of this broadened k.

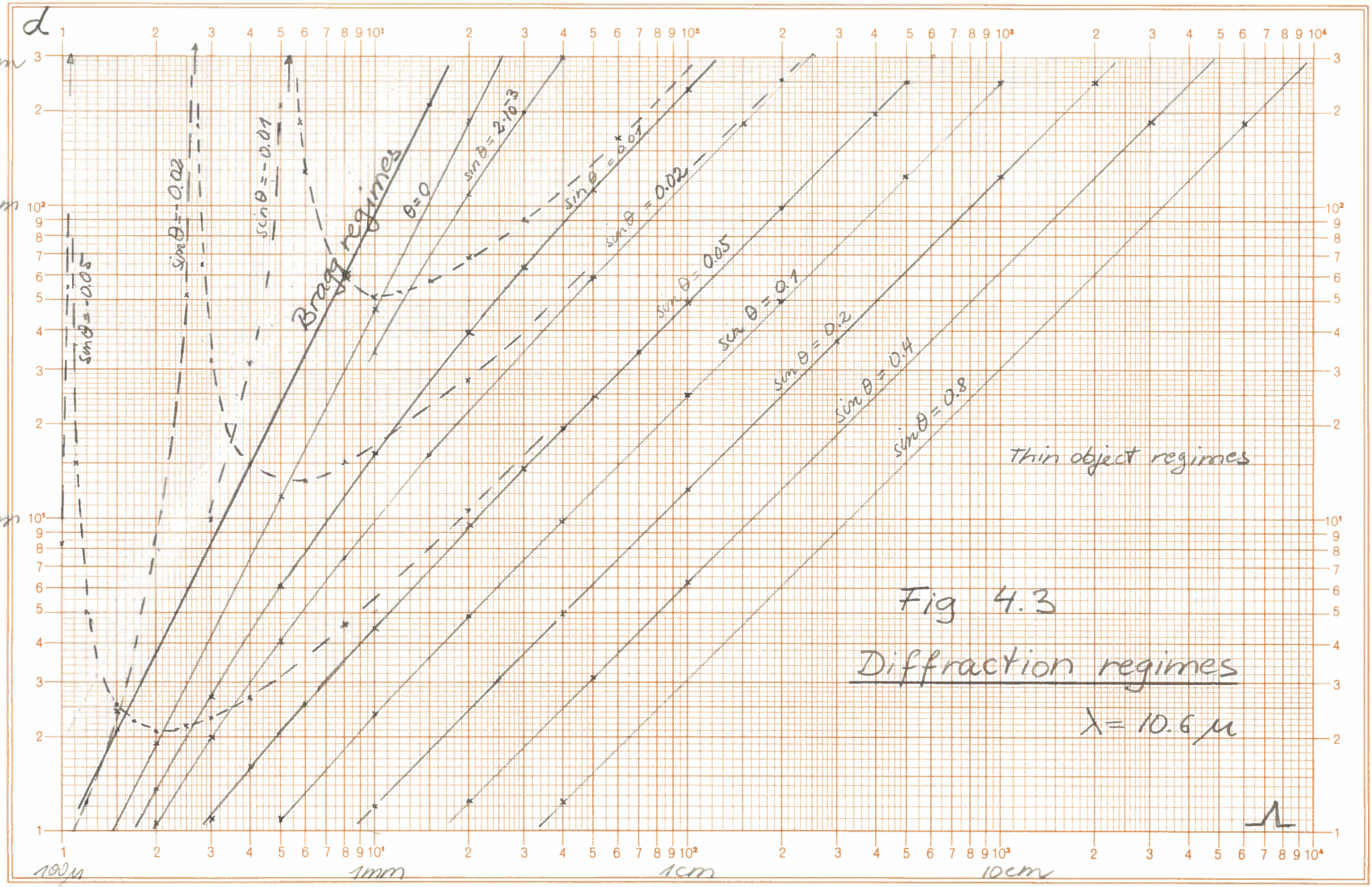

Fig 4.3

Diffraction regimes

$\lambda = 10.6\,\mu$

Logar. Teilung / Division 1-300 u. 1-10000 Einheit / Unité 62,5 mm

Ed. Aerni-Leuch, Bern, Nr. 551

V. SENSITIVITY OF OPTICAL FILTERING METHODS

We take phase contrast in the thin object regime as a representative standard case. A method rejecting one of the diffraction orders, as might be applied to thick objects, will have half its sensitivity.

The amplitude in image field is:

$$A_{(\underline{x},t)} = \sqrt{I_0}\,(1 + \varphi_{(\underline{x},t)})$$

where I_0 is the incident intensity in Watt/cm^2. We may actually consider the undiffracted field component as local oscillator field for the (homodyne) detection of the diffracted light. The intensity in the image is (from 2.11):

$$I_{(\underline{x},t)} = I_0\,(1 + 2\varphi_{(\underline{x},t)}) \qquad (5.1)$$

The L.O. photon flux incident is $\Phi_0 = I_0\,(h\nu)^{-1} = I_0\lambda/hc$, where h is Planck's constant and ν the optical frequency. The photocurrent produced by a detector of area A and quantum efficiency η is given by the number of electrons produced:

$$i_s = Ae\eta\,(1 + 2\varphi_{(\underline{x},t)})\,\Phi_0 \qquad (5.2)$$

where e is the electron charge ($e = 1.6 \cdot 10^{-19}$ AS). Since the DC component is filtered, the remaining average signal power is :

$$\langle i_{su}^2 \rangle = 4\Phi_0^2 A^2 e^2 \eta^2 \langle \varphi^2 \rangle$$

We assume that the local oscillator power is high enough to make shot noise the dominant source of noise. The shot noise power is given by

$$\langle i_n^2 \rangle = 2e\Delta f\, i_s = 2eA\eta\Delta f\,\bar{\Phi}_0$$

where Δf is the bandwidth of the receiver. The resulting signal-to-noise power ratio is

$$S/N = \frac{\langle i_{su}^2 \rangle}{\langle i_n^2 \rangle}$$

$$S/N = \frac{2A\langle \varepsilon^2 \rangle \eta \bar{\Phi}_0}{\Delta f} = \frac{\eta}{h\nu\Delta f}\langle P_{su} \rangle \qquad (5.3)$$

where $\langle P_{su} \rangle = 2A \langle \varepsilon^2 \rangle I_0$ is the useful signal power incident on the detector. This is the usual expression for the homodyne S/N ratio of an ideal reverse biased photodiode[3](Phodovoltaïc diode virtually short-circuited). For direct observation we may require $S/N \geq 3$:

$$\langle \varepsilon^2 \rangle_{min} = 3 \cdot 10^{-23} \frac{\Delta f}{\lambda A I_0 \eta}$$

or (5.4)

$$\varepsilon_{rms} \geq 5.5 \cdot 10^{-12} \sqrt{\frac{\Delta f}{\lambda A I_0 \eta}}$$

or from (2.15) :

$$\langle \Delta N^2_{(\underline{x},t)} \rangle_{min} = 3.8 \cdot 10^{2} \frac{\Delta f}{\lambda^3 A I_0 \eta}$$

or (5.5)

$$\Delta N_{rms} \geq 20 \sqrt{\frac{\Delta f}{\lambda^3 A I_0 \eta}} \quad (c.g.s)$$

According to (5.5) the sensitivity increases with increasing wavelength $S/N \alpha \lambda^3 I_0$. Hence the sensitivity in the FIR could be 10^3 to 10^4 times better than in the IR. Unfortunately the ratio of laser power available in the IR and FIR is of the same order, but in the inverse sense, so that a choice between IR and FIR has to be governed by considerations based on optical performance, convenience and cost, which seem to favor the IR option.

Numerical example

As an uper value for a detector available at CRPP (SAT photovoltaic, Hg Cd Te, $A = 6 \cdot 10^{-4}$ cm^2, $\eta \simeq 1$ (?), $\lambda = 10{,}6\mu$), let's take $AI_0 =$ 4,8 mW which is the maximum tolerable power on the element

$$\frac{\varphi_{rms}}{\sqrt{\Delta f}} \geq 2.4 \cdot 10^{-9} \text{ rad} / \text{Hz}^{1/2}$$

or

$$\frac{\Delta N_{rms}}{\sqrt{\Delta f}} \geq 8.4 \cdot 10^{6} \text{ electrons} / \text{cm}^2 \text{Hz}^{1/2}$$

In a tokamak the spectrum of drift waves is expected to lie well within a bandwidth of 1 MHz. Thus for $\Delta f = 1$ MHz.

$$\Delta N_{rms} \geq 8.4 \cdot 10^{9} \text{ electrons} / \text{cm}^2$$

As the expected wavelength of drift waves is of the order of a cm, the interaction depth will hardly be smaller than d = 5 cm. Setting $\Delta n_e = \Delta N_{rms}/d$, we get

$$\Delta n_e \geq 1.7 \cdot 10^{9} \text{ electrons} / \text{cm}^3$$

Assuming an average density $n_e = 3 \cdot 10^{13}$ cm^{-3} (tokamak), this yields a minimum detectable relative fluctuation

$$\Delta n_e / n_e \geq 5 \cdot 10^{-5} \qquad (5.6)$$

The numbers given above are for an intensity $I_0 = 8 W/cm^2$. This can be obtained by imaging a field of 15 cm diameter with a magnification m = 0.1 and a laser with 15 Watt effective power (after all losses). The detector size would limit the resolution to Λ > 5mm. If a resolution such that Λ > 0.5 mm is required, the detector size limits us to unit magnification and the sensitivity is lower by a factor of ten.

As the numbers usually cited in connection with fluctuations in tokamak plasmas are of the order of $\Delta n_e/n_e = 10^{-3}$ to 10^{-2}, the sensitivity of optical filtering methods appears to be sufficient. There is a fair chance that optical filtering might succeed event with a plasma of relatively low density, say 10^{10} - 10^{11} cm^{-3} if the level of fluctuation is high enough and concentrated in a narrow bandwidth.

If we take Δf = 10 kHz, AI_0 = 1mW, d = 5 cm we get

$$\Delta n_e \geq 4 \cdot 10^{8} \text{ cm}^{-3}$$

Additional signal processing techniques based on long time averaging may however be necessary.

VI. SUGGESTED APPLICATIONS TO PLASMA PHYSICS

6.1 Density fluctuations in a tokamak plasma

The phenomena most likely to be observed are associated with drift waves, interanl disruptions and Alfvén Wave Heating (TCA).

a) Drift waves have wavelengths of the order of the ion gyroradius [4].

$k \sim 1/r_i \sim 8\ \mathrm{rad/cm}$

$\lambda \sim 8\ \mathrm{mm}$ for TCA conditions

Microvawe measurements on TFR exhibited drift waves of total amplitude $\Delta n/n \simeq 2 \cdot 10^{-3}$. On ATC [6] values on order of magnitude higher were obtained. The plasma edge region appeared to be particularly turbulent on several machines, $\Delta n/n \simeq 50\%$, due to collisional effects [9].

a) Hasegawa's results [9] suggest that the wavelength could be as large as the region over which the plasma is collisional, typically one third of the inner radius. Consequently there is considerable interest for instruments that can detect and identify disturbances with wavenumbers down to ~ 1 rad/cm. Magnetic probe measurements on TCA [8] indicate that the drift wave spectrum extends to 200-300 kHz. The amplitudes mentioned above are well above the sensitivity limit of optical filtering methods [5.6]. The understanding of drift waves is essential to the understanding of plasma confinement.

b) The wavelength of kinetic Alfvén Waves are also closely related to the ion gyroradius. Using typical TCA parameters in their dispersion relation (with m = 2 [11]) yields $\lambda \simeq 1$ cm for Alfvén Wave Heating conditions.

On Pretext [10] Alfvén Wave Heating gave rise to relative density fluctuations of 10^{-4}, in a narrow resonant shell (3 cm, theoretical calculations). Optical filtering methods could reveal the width and location of the shell as well as damping and possibly mode conversion.

c) Magnetic islands are structures of the size of centimeters. They could be detected as they cross the field of view of the detector due to the plasma rotation (~ 10 kHz). The central region affected by an interanl disruption [5] has a larger scale, about 10 cm. Although the disruption will give rise to a detectable signal due to it's large amplitude, good imaging by the phase contrast technique would require beam diameters of ~ 30 cm. (Shadowgraphy could be tried instead).

Thus, in order to detect fluctuations of a wave-length of several cm, diffraction limited collecting optics of ~ 15 cm diameter are necessary. This is not an exhaustive list of possible applications, but a more detailed presentation of collective plasma fluctuations is beyond the scope of this report.

6.2 Comparison with conventional scattering

Optical filtering techniques have features that make them similar to microwave or CO_2 scattering methods (with which they could actually be combined) but with a widely extended range of possibilities and increased flexibility.

a) They allow the investigation of $\underline{k}$-vectors which are smaller than with ordinary scattering techniques. According to (2.13), for optics 15 cm in diameter we have

$$k_{min} = 0.7 \text{ rad/cm}$$

(Microwave scattering on TFR: $k_{min} = 4$ rad/cm [4]). This performance is made possible because the direct light which usually causes a problem, is used in our context as a local oscillator. The investigation of $\underline{k}$-vectors in this low range cannot easily be done with masks in the Fourier-plane, but by correlation measurements in the image field.

b) Correlation measurements are a new feature. We can virtually stick probes into the plasma. (detectors into it's image).
c) We have increased spatial resolution in directions perpendicular to the direction of incidence (depending on the mask used because $\Delta k \Delta x > 1$; for phase contrast see (2.2 b)). Spatial resolution in the direction of incidence is however poor.
d) High flexibility concerning the accepted domain in $\underline{k}$-space, since a mask may have any shape (holes, slits, annuli ...).
e) The sensitivity may be higher or lower than for ordinary scattering depending on the object. A plane wave is "very concentrated" in $\underline{k}$-space, so that ordinary scattering is more sensitiv. On the other hand we may have objects that are "concentrated" in real space (and thus "diluted" in $\underline{k}$-space) like magnetic islands and resonant layers. Here imaging is superior.

6.3 Monitoring of fluctuation levels

When no selection of scattering angles is made, the full frequency spectrum associated with the band of the instrument (k typically between 1 and 100 rad/cm) is obtained with maximum spatial resolution. See Fig. A1.1 for an example.

In addition to a spectrum analyzer a bank of bandpass filters followed by square law devices and lawpass filters could be used, which monitor the temporal variations of fluctuation levels during a discharge, in selected frequency bands. (The sensitivity of such a system is roughly the same as for direct observation (5.4), with Δf replaced by the geometric mean of the bandwidth of the input filter and the output filter).

6.4 Dispersion relations

The use of a mask with an array of holes or slits in the Fourier plane (see Fig. A1.3) may permit under certain conditions to establish a dispersion relation. As with microwave scattering, errors can arise from the $k/\cos\theta$ uncertainty (when diffraction does not occur in the Bragg regime (4.13)), from a non-homogeneous plasma or non-linear behaviour of the waves.

Since homodyne detection is used, dissymetries of the ω-spectrum will not be revealed. This drawback can be overcome by correlation measurements. Discrimination between radial and azimuthal behaviour seems also possible.

6.5 Quantitative work

In the thin object case (phase contrast), the photocurrent fluctuations are related to the refractive index fluctuations by

$$\Delta i/i = 2\pi \Delta n \, d/\lambda$$

where

$$\Delta n = \frac{e^2 \lambda^2 \Delta n_e}{2\pi m_e c^2} \qquad (6.1)$$

Thus we obtain the electron density fluctuations if the interaction depth is known. Taking d equal to the plasma thickness might give an underestimation of the local value.

In the ideal case of scattering from a uniform, homogeneous, stationary and infinite plasma, optical filtering can provide the differential scattering cross section for $\underline{k} \sim \perp \underline{k}_0$.

$$\frac{d\Sigma}{d\omega d\Omega} = \left(e^2/m_e c^2\right) S(\underline{k},\omega)$$

where

$$S(\underline{k},\omega) = \frac{V}{2\pi} \langle |n_e(\underline{k},\omega)|^2 \rangle \qquad [7]$$

We may use a mask with only a hole for order 0 and one for the $\underline{k}$ vector of interest with width Δk related to $\Delta\Omega$. The square average of the relative photocurrent fluctuations is then equal to the cross section for an effective volume

$$V = Ad/m^2$$

where A is the detector area
d the spatial depth of the plasma
m the magnification of the imaging system

As only $\underline{k}$ vectors $\sim \perp \underline{k}_0$ (fixed) are explored, the computations of the total fluctuation level relies on additional symmetry assumptions.

When no selection in $\underline{k}$-space is used (phase contrast), the total scattering cross section for $|\underline{k}| > k_c$ can be obtained in a single measurement.

6.6 Aspects of the application to TCA

a) Collection optics

To achieve good performance at low $\underline{k}$, we propose diffraction limited collection optics of 15 cm diameter or more. Such an element is best diamond machined as off-axis parabolic mirror (elliptic if divergent illumination is used).
Cost: 7000 SF (AERO RESEARCH ASSOCIATES)

b) Expanding optics

In the cheapest version a focussing lens and a spatial filter would be used. The beam would expand by propagation over 5-10 m. A more compact version would need an additional diffraction limited off axis mirror in order to produce a parallel incident beam.

c) Imaging optics

As high resolution in real space is probably not required, the lens performing the inverse transform can relatively cheap and small.

d) Windows

Since the whole plasma should be accessible, the elongated (390 x 70 mm) windows on TCA appear suitable. Their narrow lateral width does not seem to be a serious disadvantage because k-vectors are (expected to be) perpendicular to the magnetic field lines. Two windows would cost ~ 15 000SF for ZnS and ~ 30 000 for ZnSe (SCHOTT).

e) Phase plate

This can be made with no or little cost either with a Mylar film (see appendix A.1) or controled vacuum deposition of a metal layer of adequate thickness on a mirror or flat. (The result should be termed "phase mirror").

f) Detectors

A suitable nitrogen cooled photovoltaïc detector is available at CRPP. An additionnal one would cost a few 10^4 SF. An array with 10-20 elements would cost 100 000-150 000SF (ORIEL).

g) Laser

First experiemnts could be carried out with lasers available at CRPP or EPFL. A commercial CO_2 laser with a few lens of Watts output power costs about 50 000 SF.

Remark

To allow easy scanning of the plasma without adjustment of the optics a trolley similar to the one used for the Thomson scattering diagnostic would be ideal. In a first step expensive investment should however be avoided. Preliminary results obtained with a "cheap" version (using KCI lenses 10 cm in diameter - 1 200 SF) with fixed optics would provide sufficient information optimaly design a definitiv version, and avoid costly errors.

REFERENCES

1 Jack D. Gaskill, Linear Systems, Fourier Transforms, and Optics Wiley, 1978

2 Born and Wolf

3 M.C. Teich, Infrared Heterodyne Detection, Proc. IEEE 56 (1), 37 -46 (1968).

4 F. Koechlin, V. Glaude, J. How, Mesure d'instabilités dans un plasma chaud et dense par diffusion d'ondes millimétriques EUR-CEA-FC-871 (Fontenay 1977).

5 The T.F.R. Group, Electron temperature and density relaxations during internal disruptions in TFR tokamak plasmas, Plasma Physics, Vol. 19, (Pergamon 1977).

6 R.J. Bickerton, Survey of tokamak experiments, Culham Laboratory, 1977.

7 Lovberg, Griem (editors), Methods of experimental physics 9-A.

8 P.A. Duperret, Travail pratique, été 82.

9 A. Hasegawa, Oral presentation at CRPP, 27.10.82

10 R.D. Bengtson et al. Alfvén Wave Heating in PRETEXT (Grenoble 82).

11 Antoine Pochelon, CRPP, Personal Communication.

12 P.D. Morgan, Optical refractivity studies on plasma focus, Royal Holloway College 1974.

13 H. Weisen, Travail de diplôme, CRPP, 1981.

14 H.M. Presby and D. Finkelstein, Plasma phasography, The Review of Scientific Instruments Vol. 38, No 11, 1967.

APPENDIX 1

Experiment with an air jet as object

An air jet streaming out of a nozzle 4 mm in diameter was taken as an object in the following setup :

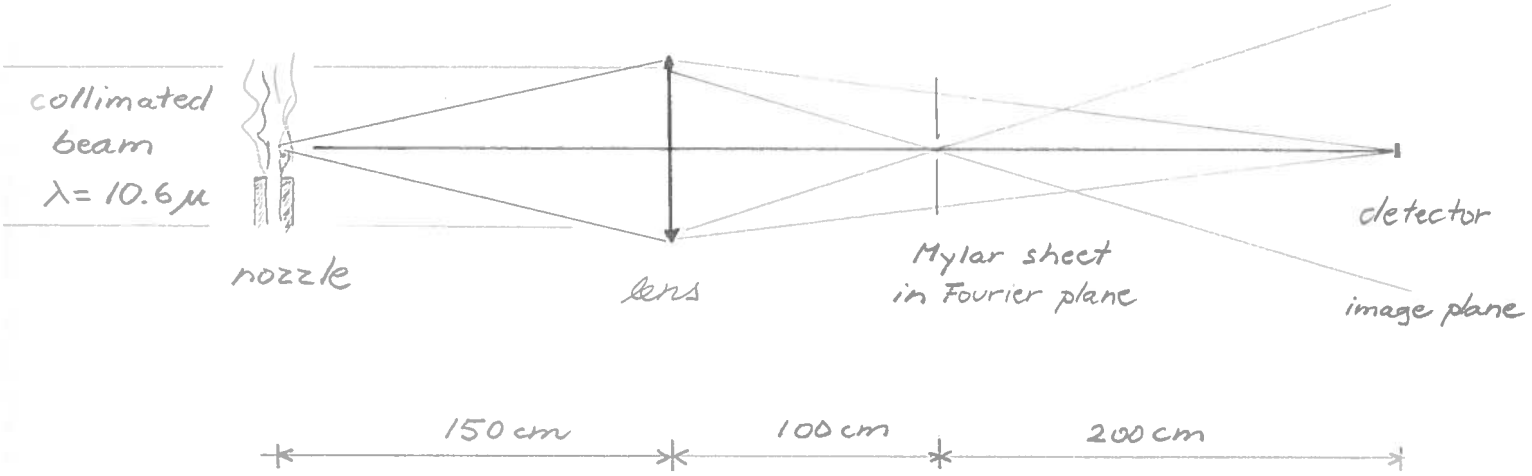

The lens (f = 100 cm) produced simultaneously the image of the source in the Fourier plane and an image of the jet at the detector plane. The "phase plate" was a MYLAR sheet of 2.5 μ thickness causing the diffracted wave to be retarded by ~ 1,3 radians (instead of 1.57). The laser burnt itself the hole for order 0 about 2 mm in diameter. This corresponds to a lower cutoff frequency of 6 rad/cm.

The setup has a magnification of 2. The total IR power in the image field was about 8 W over an area of ~ 64 cm^2. This yields an local oscillator power of ~ 0.1 mW at the photovoltaic diode. According to (5.4) the sensitivity should permit detection of phase shifts down to 10^{-6} radians when the bandwidth is 1 kHz.

The detector was a HgCdTe photovoltaic diode of 0.14 mm radius manufactured by SAT.

Results

An oscillatory signal at ~ 50 kHz corresponding to phase fluctuations = $2 \cdot 10^{-2}$ was first observed. The signal was spectrum analyzed and usually showed several discrete modes and a continous background extending to about 400 kHz. The diode was effectively short circuited by a current-to-voltage converter with a flat response up to 1 MHz. Fig. A1.1 shows typical spectra obtained with phase contrast, simple imaging and with the jet turned of (overall noise).

The signal without a filter can be explained by out-of-focus contributions, aberrations, unequal diffraction in orders ± 1. At low frequencies (and thus low $\underline{k}$ vectors) phase contrast brings consideralbe improvement, but fails at frequencies above ~ 200 kHz. From the dispersion relation of sound waves this is seen to correspond to wavelength of ~ 0.3 mm. From Fig. (4.3) with d = 4 mm we find this to correspond to the limit of depth of focus. Thus for frequencies above 200 kHz the thin object model is invalid.

Fig. A1.2 shows the spectrum with a linear scale. The cutoff at ~ 30 kHz corresponds well to k_c = 6 rad/cm. This corresponds to wavelength of 1 cm or a quarter of the beam diameter and is a factor of 3 less than the diffraction limit given by (2.13). Possible explanations are lens aberrations and the fact that the laser burns a hole somewhat larger than necessary.

The observed noise level is higher than expected, particularly at low frequencies. If the mode at 50 kHz of Fig. A1.1 is taken as a reference ($\varphi \cong 2 \cdot 10^{-2}$ rad), the overall noise level at high frequencies limits sensitivity to 10^{-5} radians, 10 times less than the theoretical value. Possible explanations are laser output fluctuations, low quantum efficiency, other noise sources than shot noise.

A mask with an array of 11 holes with diameter 1 mm and 2 mm spacing was introduced in the Fourier plane. $\underline{k}$-vectors were found to be mainly parallel to the jet when the mask was turned. Fig. A1.3 was obtained with the array parallel to the jet and Fig. A1.4 with all but the second pair of holes and the central hole obstructed. These spectra should permit to obtain the dispersion relation of sound waves in air. We got however systematically the value of 240 m/s for the speed of sound. A previous setup had given a better agreement. Possible explanations are errors in calibration or perhaps the $k/\cos\theta$ undetermination.

The experiment should be carried out once more with more carefull calibration, measurement of noise, etc. The use of a simpler object, like monochromatic ultrasonic wave produced by a transducer, or a surface wave device would be an advantage.

Comparison with Kolmogorov spectrum

We may interpret the uniform region above 100 kHz of the spectrum A1.1 as the essentially isotropic inertial subrange where kinetic energy cascades down to smaller eddy sizes (larger k-vectors) by vortex stretching, viscous dissipation being negligible. The spectral energy density, which is proportional to the spectral density of the refractive index, is given by the 3-D Kolmogorov spectrum:

$$\langle \Delta\tilde{n}^2_{(\underline{k})} \rangle \sim \langle \tilde{\varphi}^2_{(\underline{k})} \rangle \sim |\underline{k}|^{\alpha}$$

where $\alpha = 11/3$

This dependency has been found from the range between the two arrows of Fig. A1.1 $|\underline{k}|$ was obtained from $|\underline{k}| = \omega/v_{sound}$. A least squares fit over six points (Fig. A1.5) shows surprising agreement:

$$\alpha = 3{,}67 \pm 0{,}10$$

FIG. A1.1

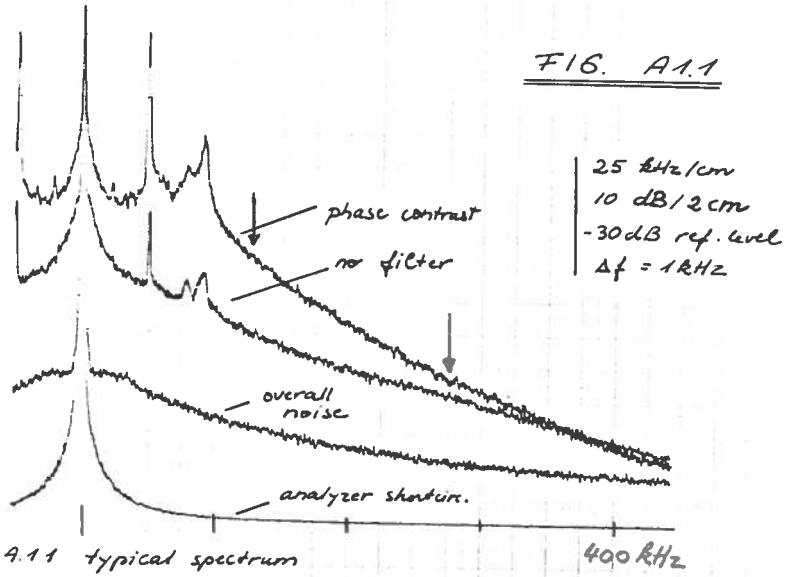

A.1.1 typical spectrum

FIG. A1.2

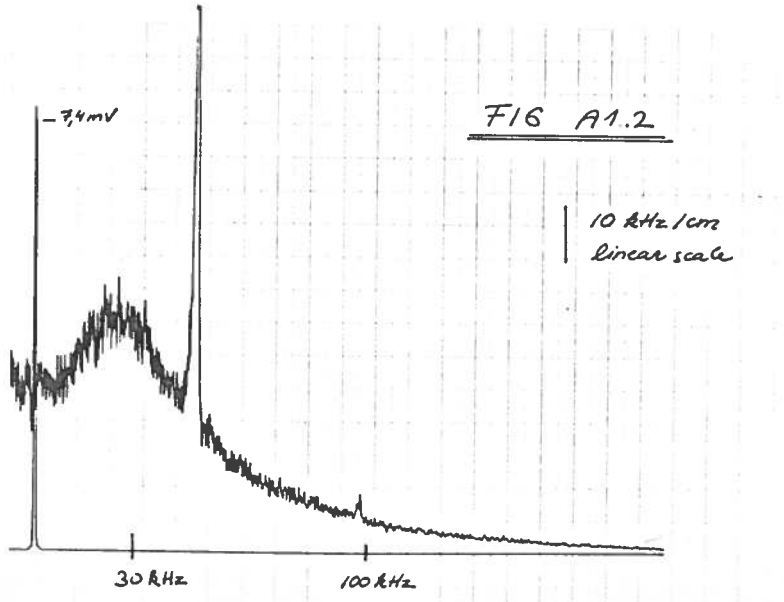

FIG. A1.3

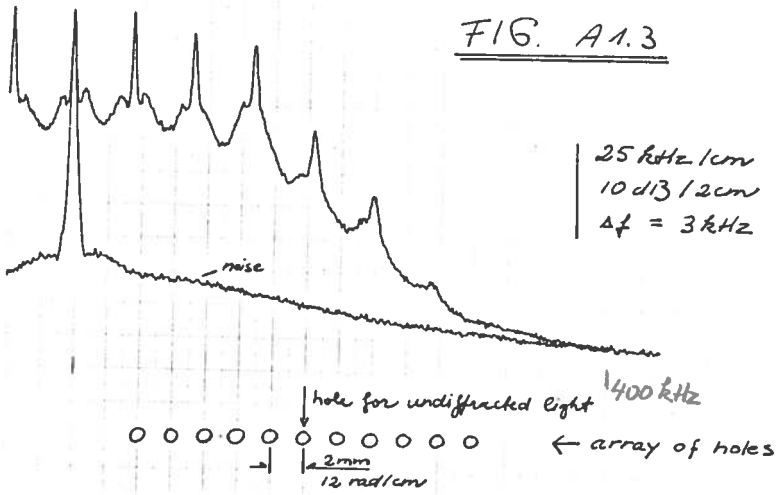

Spectrum obtained with selection of diffraction angles

FIG A1.4

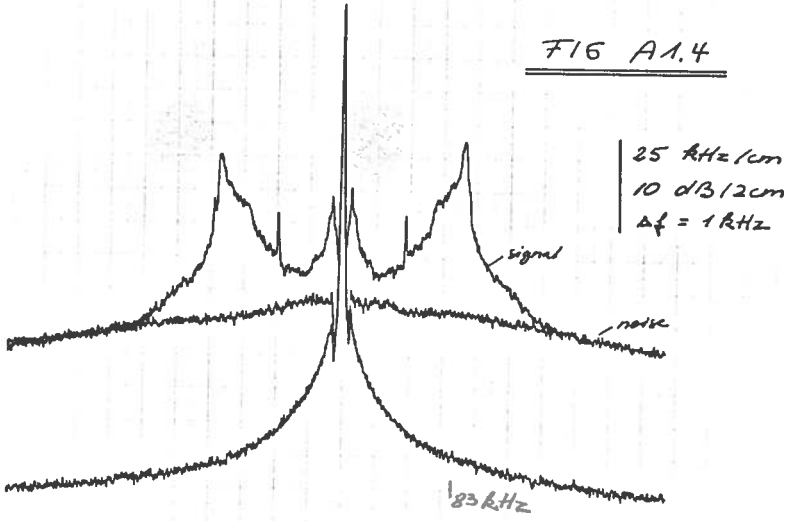

Second hole pair only. $k = 24$ rad/cm $\Delta k = 6$ rad/cm

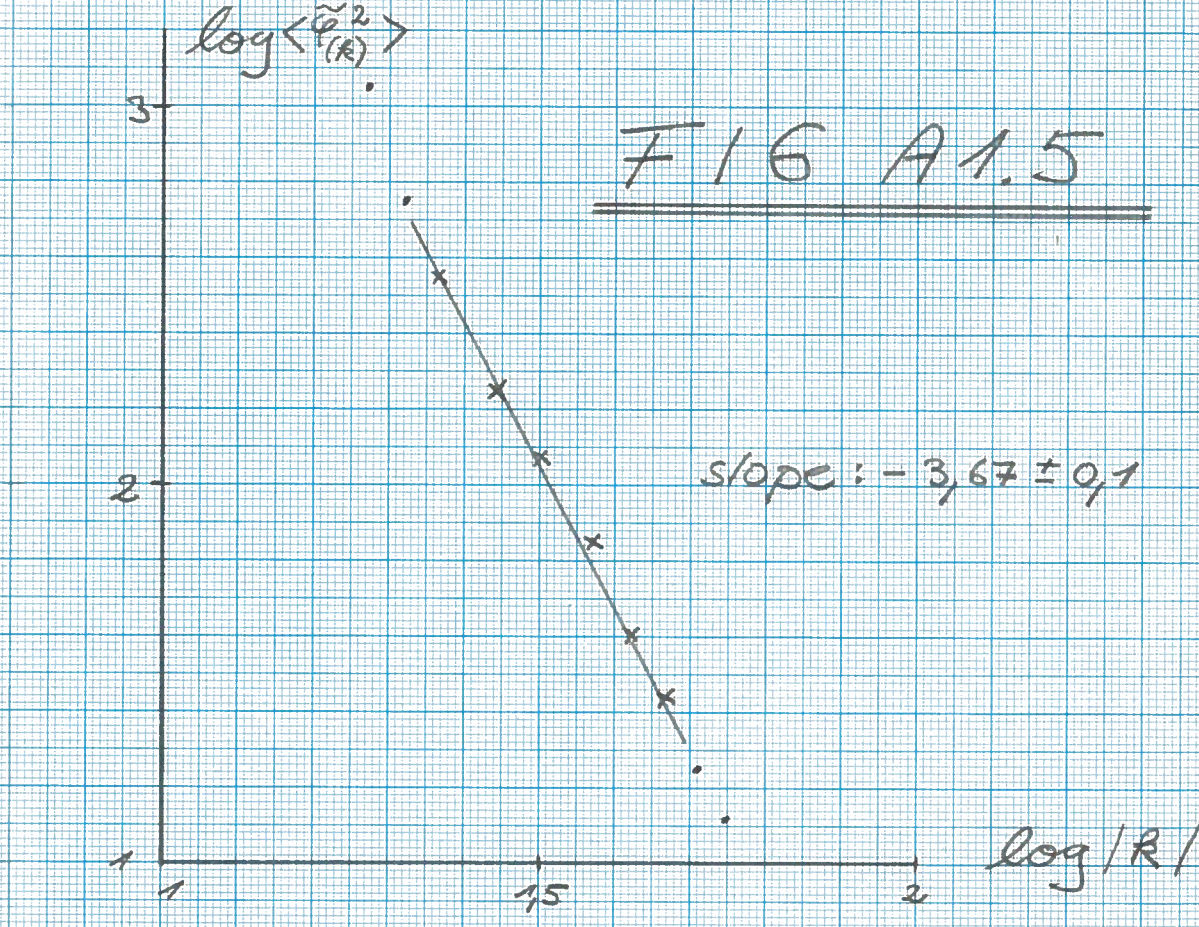

F16 A1.5

Comparison with Kolmogorov spectrum